the FEBS Journal

# Electrostatic contacts in the activator protein-1 coiled coil enhance stability predominantly by decreasing the unfolding rate

Jody M. Mason

Department of Biological Sciences, University of Essex, Colchester, UK

**Keywords**
activator protein-1; coiled coils; electrostatic interactions; protein design; protein folding

**Correspondence**
J. M. Mason, Department of Biological Sciences, University of Essex, Wivenhoe Park, Colchester, Essex CO4 3SQ, UK
Fax: +44 1206 872 592
Tel: +44 1206 873 010
E-mail: jmason@essex.ac.uk

(Received 2 September 2009, revised 9 October 2009, accepted 15 October 2009)

doi:10.1111/j.1742-4658.2009.07440.x

The hypothesis is tested that Jun–Fos activator protein-1 coiled coil interactions are dominated during late folding events by the formation of intricate intermolecular electrostatic contacts. A previously derived cJun–FosW was used as a template as it is a highly stable relative of the wild-type cJun–cFos coiled coil protein (thermal melting temperature = 63 °C versus 16 °C), allowing kinetic folding data to be readily extracted. An electrostatic mutant, cJun(R)–FosW(E), was created to generate six Arg-Glu interactions at $e$–$g'+1$ positions between cJun(R) and FosW(E), and investigations into how their contribution to stability is manifested in the folding pathway were undertaken. The evidence now strongly indicates that the formation of interhelical electrostatic contacts exert their effect predominantly on the coiled coil unfolding/dissociation rate. This has major implications for future antagonist design whereby kinetic rules could be applied to increase the residency time of the antagonist–peptide complex, and therefore significantly increase the efficacy of the antagonist.

## Introduction

The primary factors governing protein–protein interaction stability have yet to be fully elucidated. To this end, our focus continues on the coiled coil region of the activator protein-1 (AP-1) transcription factor. Coiled coils are one of the more tractable examples of quaternary structure [1–4] and are highly ubiquitous protein motifs found in 3–5% of the entire coding sequence [5]. An additional appeal in studying the mechanisms of association lies in the fact that AP-1 is known to be oncogenic, and indeed is upregulated in numerous tumours. Numerous signalling pathways converge on AP-1, thereby controlling gene expression patterns and resulting in tumour formation, progression and metastasis [6–9], in addition to bone diseases, such as osteoporosis, and inflammatory diseases, such as rheumatoid arthritis and psoriasis [10–12]. Clearly, the design of highly stable coiled coil structures using design rules is of general interest to the protein design community. In addition, understanding the molecular mechanism of protein association/dissociation is fundamental in lead design and synthesis of peptide-based antagonists that aim to bind and sequester proteins that are behaving abnormally. Often, the most rational place to begin in peptide-based antagonist design is to use one wild-type binding partner as the design scaffold. There are additionally several key advantages in using peptides and peptide mimetics over conventional small molecule-based approaches [13–15] as starting points in therapeutic design, because they are less likely to be toxic than small molecule inhibitors as they are able to be degraded over time. They will probably be able to inhibit protein–protein interactions in which

**Abbreviations**
AP-1, activator protein-1; bCIPA, basic coiled coil interaction prediction algorithm; DHFR, dihydrofolate reductase; PCA, protein fragment complementation assay; $T_m$, thermal melting temperature.

the interface is large. In addition, peptides are much less likely to be immunogenic when short (12 residues or less), as they fall below the threshold of immunogenic proteins and can be readily modified to deal with protease susceptibility issues, and to optimize the lipid–water partition coefficient (logP) required for membrane permeability.

Therefore, peptide mimetics offer a tangible opportunity to inhibit protein–protein interactions and therefore prevent and sequester proteins involved in pathogenic events. For example, the coiled coil 'fusion inhibitor' Fuzeon® peptide (enfuvirtide) has been generated by Trimeris and Roche for use in patients who have multidrug-resistant HIV. It works by forming a coiled coil with the heptad repeat 1 domain of gp41, thereby preventing CD4 cells from fusing with HIV and becoming infected [16,17]. Until recently, research has largely focused on small molecule inhibitors, but the potential of using peptides as the starting point in the generation of therapeutics is now a growing area [18,19]. Peptides harbour the potential for chemical and biological diversity while maintaining high specificity and affinity for a protein target.

## Previously selected pairs

Protein–protein interactions capable of sequestering oncogenic Jun–Fos AP-1 leucine zipper proteins were previously generated using genetic libraries containing partially randomized oligonucleotides [20–22]. These libraries retained the vast majority of wild-type parent residues, with electrostatic options at *e/g* positions and hydrophobic options at *a* positions, known to conform to coiled coil structures (Fig. 1). In particular, this approach made use of protein fragment complementation assays (PCAs), in which libraries were genetically fused to one half of an essential split dihydrofolate reductase (DHFR) enzyme, with a target peptide (i.e. cJun or cFos) fused to the second half, and with bacterial DHFR inhibited using trimethoprim [20,23]. Library members that bound to their target brought DHFR fragments together, rendering the enzyme active, and promoting cell growth. This *in vivo* screen removed unstable, insoluble or protease-susceptible peptides and was followed by growth competitions to select a single sequence conforming to the tightest binding interaction. Assay 'winning' peptides, termed JunW and FosW, generated dimers with thermal melting temperature ($T_m$) values of 63 °C (cJun–FosW) and 44 °C (JunW–cFos) compared with only 16 °C for wild-type cJun–cFos [20], with differences analysed against sequence changes. Known homologues (JunB, JunD, FosB, Fra1 and Fra2) were synthesized for analysis, extending the number of interactions from 10 to 45, permitting a rigid interpretation in distinguishing interacting from noninteracting proteins. One

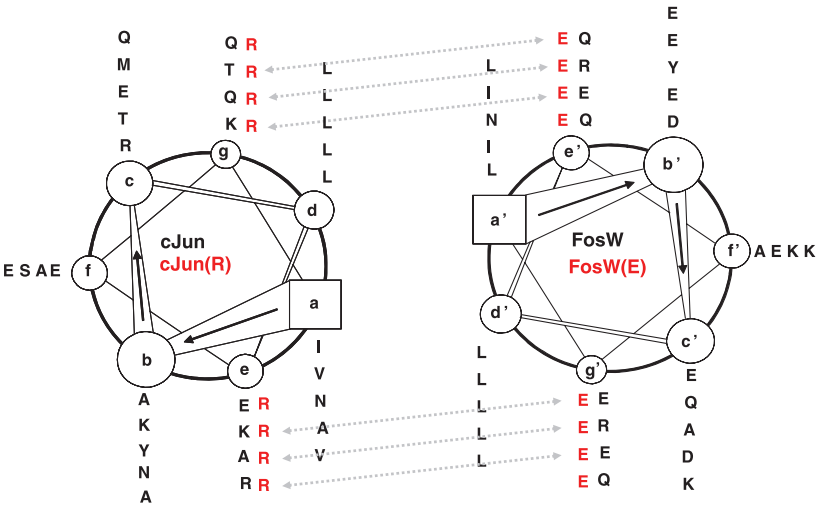


**Fig. 1.** Schematics of library designs. The helical wheel diagram looks down the axis from the N-terminus to the C-terminus. Heptad positions are labelled *a* to *g* and *a'* to *g'* for the two helices, respectively. For simplicity, supercoiling of the helices is not shown. Residues *a* and *d* make up the hydrophobic interface, whereas electrostatic interactions are formed between residue *i* (*g* position) and *i'* + 5 (*e* position) within the next heptad. A polar Asp pair at *a3–a3'* is maintained to direct specificity and to correct heptad alignment [27]. Shown in black are the residues for the previously selected FosW–cJun pair. This pair forms the template for the electrostatic mutant, cJun(R)–FosW(E). This mutant has all *e* and *g* positions of FosW replaced with Glu (red) and all *e* and *g* positions of cJun replaced with Arg (also red), with the remaining residues unchanged. The cJun(R)–FosW(E) pair has been designed to probe further the role of electrostatic residues in the kinetics of association and folding, and to overall stability.

outcome of this study was the finding that α-helical propensity was an important and largely overlooked third parameter in designing dimerization competent structures. Consequently, a basic coiled coil interaction prediction algorithm (bCIPA) was written to predict $T_m$ values for parallel dimeric coiled coils from sequence data input alone [20], taking into account core, electrostatic and helical propensity contributions. This created an effective method that is much more straightforward than others to date [20].

## AP-1 folding

Further insight into the structural determinants of stability arose by dissecting the folding pathway of four Jun-based leucine zipper variants that bind with high affinity to cFos [24]. This encompassed a PCA-selected winner (JunW [20]) and a phage display-selected winner ($JunW_{Ph1}$ [25]), as well as two intermediate mutants, owing to the fact that the two enriched winners differed from each other in only two of 10 semi-randomized positions (with $\Delta T_m$ values of 28 and 37 °C over wild-type). cFos–JunW, cFos–$JunW_{Ph1}$ and both intermediate mutants (cFos–$JunW_{Q21R}$ and cFos–$JunW_{E23K}$) displayed biphasic kinetics in the folding direction, indicating the existence of a folding intermediate. In this study, it was ascertained that the first reaction phase was fast and concentration dependent, showing that the intermediate was readily populated and dimeric. The second phase was independent of concentration (consistent with a unimolecular reaction) and exponential. In contrast, in the unfolding direction, all molecules displayed two-state kinetics. Collectively, this implied a transition state between denatured helices and a dimeric intermediate that is readily traversed in both directions. The added stability of cFos–$JunW_{Ph1}$ relative to cFos–JunW was achieved via a combination of kinetic rate changes; although cFos–$JunW_{E23K}$ had an increased initial dimerization rate, prior to the major transition state barrier, cFos–$JunW_{Q21R}$ displayed a decreased unfolding rate. Although these data were based only on single point mutations, taken collectively the former suggest that improved hydrophobic burial and helix-stabilizing mutations exert their effect on the initial, rapid, monomer collision event, whereas electrostatic interactions appear to exert their effect late in the folding pathway. Establishing that this is the case in general will open vast possibilities to designing increased stability protein–protein interactions that either associate/fold rapidly, dissociate/unfold slowly or achieve their increased stability (relative to the parent protein) by a combination of these two kinetic changes.

## Electrostatic folding determinants

Peptides that associate and dissociate rapidly probably generate similar overall equilibrium stabilities as those that associate and dissociate slowly, but would have quite different implications for *in vivo* function. This would in turn have large implications for protein design strategies. To this end, we describe a robust test of enhanced intermolecular electrostatic contacts within the Jun–Fos AP-1 system. Explicitly, both association/folding and dissociation/unfolding events are monitored using multiple enhanced electrostatic contacts based on a related previously selected peptide, cJun–FosW. cJun–FosW is known to display particularly high interaction stability ($T_m$ = 63 °C). The dimeric pair was constructed to analyse the contribution to kinetic and thermodynamic stability made from an all Arg-Glu *e/g* electrostatic complement [26] between the two helices. By robustly establishing the contribution that these residues make to the identifiable steps in the folding pathway, it is anticipated that this information can be used as an easy system for lead design and synthesis, with the ultimate aim of designing stable and effective peptidomimetic antagonists that can bind to the dimerization motif of specific AP-1 pairs, and inhibit their function. For example, it could be possible to change the stability of the dimeric structure by accelerating the association/folding rate (these processes are concomitant) and decreasing the dissociation/unfolding rate. Thus, the ultimate outcome would be the design of a complex that is able to form quickly and, once formed, will display very slow off rates, thus greatly accelerating the design of effective protein–protein interactions.

## Results

To investigate the contribution made by electrostatic residues to the folding pathway, the thermodynamic and kinetic contribution to stability made by six engineered Arg-Glu *e/g* pairs in one dimeric pair [cJun(R)–FosW(E)] was investigated (see Tables 1 and 2). The stability changes were measured relative to a stable cJun–FosW peptide (see Fig. 1) that served as a scaffold in the design process and that had been previously selected using PCA [20]. Both dimeric peptide pairs were 37 residues in length and contained 4.5 heptad repeats. The dimers also retained an Asn-Asn pair, to generate a hydrogen bond between positions *a3–a3′*, ensuring that heptads were correctly aligned, orientated and favoured dimer formation over alternative oligomeric states [27]. The electrostatic pair, cJun(R)–FosW(E), contained only Arg residues within all *e/g*

positions of cJun and only Glu residues within *e/g* positions of FosW. The mutant was designed to test an earlier finding suggesting that electrostatic contacts are formed rather late in the folding pathway and therefore exert their effect on the unfolding rate of preformed pairs [24]. In creating a mutant that contained multiple *e/g* Arg-Glu pairings, dimers were designed that, if correct, should enhance the effects of earlier findings, thus reinforcing our conclusions and allowing us to continue with further rounds of design based on these results.

## Equilibrium stability

The parent cJun–FosW peptide displayed a $T_m$ of 63 °C [20]. Rather surprisingly, the cJun(R)–FosW(E) mutant could barely be denatured at 20 μM total peptide concentration, with a $T_m$ of 82 °C (this required using a restrained fit on the upper baseline – see Fig. 2 and Table 2). Thus, it would appear that complementary charged residues are able to collectively confer very high overall stability. This is in contrast to data published from the Krylov group [29], which were used to directly compare the differences in energetic contributions for the six electrostatic residue contacts relative to the original cJun–FosW peptide (see Table 3). Indeed, for the electrostatic mutant, only approximately 3.8 kcal·mol$^{-1}$ of additional stability was predicted to be introduced into the molecule based on these data. Running these sequences through bCIPA [20] or the base optimized weights algorithm of Fong *et al.* [28] generated $T_m$ values and stability rankings, respectively, that were in very close agreement with the experimental data (see Table 2). bCIPA works by considering core *a–a′* pairs, electrostatic $g_i$–$e'_{i+1}$ and $e_{i+1}$–$g_i'$ pairs, as well as helical propensity factors, and gave a score of −1.5 kcal·mol$^{-1}$ for Arg-Glu electrostatic pairs (QQ≈KE≈RE = −1.5; KQ≈RQ = −1; KD≈RD≈EQ = −0.5). Its parameters also oppose charge pairings by imposing energetic penalties (DD≈DE≈EE≈RR≈KK≈RK = +1). In all cases, bCIPA treats $g_i$–$e'_{i+1}$ and $e_{i+1}$–$g_i'$ energetic pairs as the same for simplicity [20]. As such, bCIPA considers electrostatic changes to make cumulatively large contributions to overall stability, and thus makes a good estimate of overall stability. Similarly, base optimized weights consider $d_id'_i$, $a_ia'_i$, $a_id'_i$, $d_ia'_{i+1}$, $d_ie'_i$, $g_ia'_{i+1}$ and $g_ie'_{i+1}$ pairings [28], but do not consider α-helical stability as a direct contributing factor. It would therefore appear that the contribution estimated by Krylov and coworkers [29] was somewhat underestimated. Indeed, the electrostatic mutant was of higher stability ($\Delta T_m$ = 26 °C at 20 μM) than predicted for the introduction of these residues.

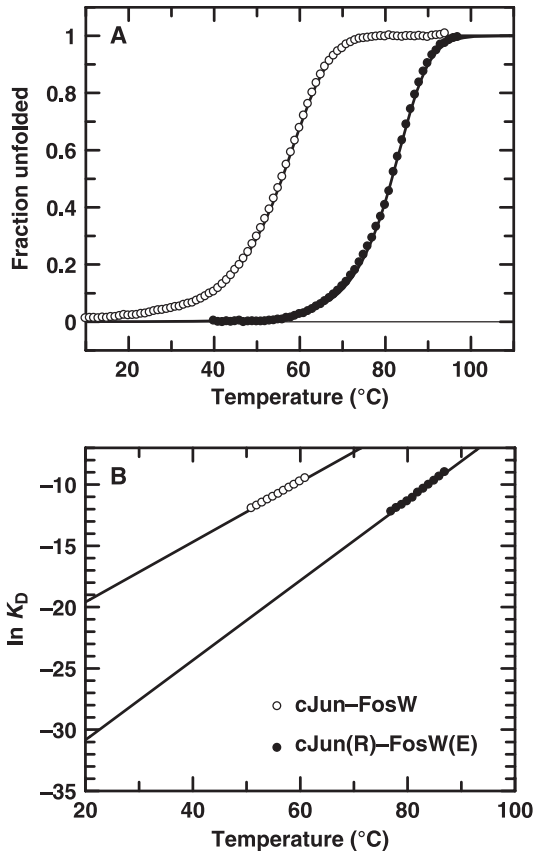


**Fig. 2.** Thermal denaturation profiles. (A) Denaturation profiles for AP-1 variants were designed to test the energetic contribution of 'electrostatic' residues to the stability of AP-1 leucine zippers. Shown is the cJun–FosW coiled coil (empty circles) on which the electrostatically stabilized coiled coil (filled circles) was based (see also Table 3). The total peptide concentration for both dimers was 20 μM. Both fits to the two-state model (Eqn 2) agree well with measured data. (B) Linear fit to the transition zone of data shown in (A) to determine $K_D$ at 293K (derived data shown in Table 2). The correlation coefficients ($r$) for the two linear fits are 0.9991 and 0.9998. Experiments were undertaken in a 1 cm CD cell, and overall ellipticity was monitored at 222 nm. $\Delta G$ values obtained from thermal melting data were normalized to be independent of peptide concentration (see [24]). Only data from around the midpoint of the transition (where the S/N ratio is greatest) were used to give the most reliable $K_D$ estimate.

The observed $\Delta\Delta G$ of −6.6 kcal·mol$^{-1}$ was almost 3 kcal·mol$^{-1}$ more than the −3.8 kcal·mol$^{-1}$ predicted from the Krylov *et al.* data. Because bCIPA accounts for *e/g*, core and propensity terms, the indication is that a rather more sizeable contribution to interaction stability is made by these electrostatic residues than has been previously predicted. In addition, the high helical propensity that was predicted for the selected FosW peptide (46% average across the peptide) was not matched by any homologues (4–12% predicted; [30–32]), indicating

that in this study, helicity was not a major determinant in overall interaction stability. One might predict that the co-operative nature of forming multiple salt bridges also contributes to the increased stability of cJun(R)–FosW(E). However, bCIPA does not make this assumption and arrived at a $T_m$ that was very close to that observed (94 °C versus 98 °C; see Table 2). Other possible reasons for the discrepancy in observed and estimated stability based on the Krylov *et al*. data could be due to the sequence context of the introduced residues as well as the unknown contribution that the *e4–g′3* Gln-Thr pair makes to coiled coil stability in the parent cJun–FosW molecule (see Table 3, Fig. 1).

### Stopped-flow CD folding studies

No kinetic data could be extracted for the wild-type cJun–cFos complex, even at high concentrations and low temperatures [24], due to overall low stability ($T_m$ = 16 °C [20]). However, both mutants in this study displayed high stability and kinetic data were readily extracted. The mutants were fitted for both two-state ($2U = F_2$) and three-state ($2U = I_2 = F_2$) models in folding and unfolding directions, and the best fits were taken based on the residuals for each. The fits collectively imply that folding and unfolding comprise two transitions in either direction. The height of one transition state, relative to the other, dictates whether one or two phases are observed. Under experimental conditions, two phases were observed in the folding direction, informing that the first transition state in folding is of a lower energy. Indeed, two folding phases and one unfolding phase were observed for cJun–FosW. If the first transition state is large relative to the second, one would predict one detectable folding phase and two unfolding phases. However, if the transition states are comparable in height, one would predict two folding phases and two unfolding phases [cJun(R)–FosW(E)]; thus, all properties of the reaction can be monitored. It should be noted, however, that the complex kinetics could also be due to the transient formation of homodimers prior to the formation of the heterodimer, and that this possibility cannot be ruled out.

### Native gel electrophoresis

Native gel electrophoresis was applied to confirm that the cJun–FosW and cJun(R)–FosW(E) species formed were dimeric (Fig. 3). In this experiment, gels lacking SDS were loaded with concentrated protein samples so that fully folded peptides could migrate according to their overall charge at low pH. This in turn allowed homomeric complexes to be distinguished from those that were heteromeric. Indeed, FosW–cJun (lane 3) appeared as an average of its constituents, FosW (lane 1) and cJun (lane 2). Likewise, cJun(R)–FosW(E) (lane 6) also clearly formed a heterotypic complex of 1 : 1 stochiometry, as it appeared as the average of its constituents, FosW(E) (lane 4) and cJun(R) (lane 5).

### cJun–FosW

The folding transients of the parent molecule cJun–FosW contained two detectable folding phases and one unfolding phase, consistent with our previous studies on cFos–JunW-based dimers [24]. In the folding direction, the first of these transitions was slightly faster ($5.8 \times 10^6$ $M^{-1}s^{-1}$, equivalent to a $k_{app}$ of 166 $s^{-1}$; see Table 1) compared with the cFos–JunW

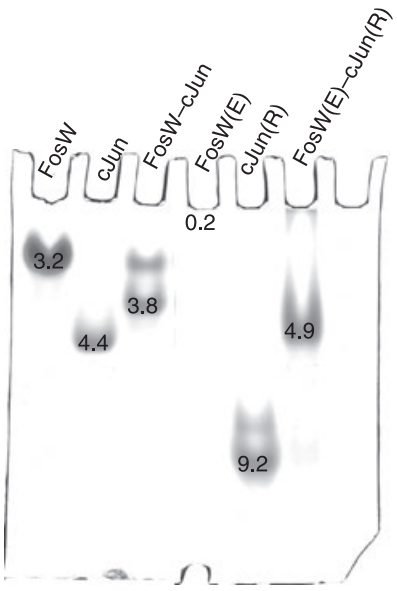


**Fig. 3.** Native gel PAGE. The native gel was created using total peptide concentrations of 480 μM, undertaken at pH 3.8 and at 4 °C and demonstrates species that have been designed to form heterotypic complexes. At this pH all peptides are positively charged and migrate towards the cathode. FosW–cJun (charge +3.8, lane 3) appears as an average of its constituents, FosW (charge +3.2, lane 1) and cJun (charge +4.4, lane 2) showing that it is heterodimeric. FosW(E)–cJun(R) (charge +4.9, lane 6) also clearly forms a heterodimeric complex, as it is distinct from its constituents, FosW(E) (charge +0.2 – barely migrated into the gel, lane 4) and cJun(R) (charge +9.6, lane 5). In addition, from the differences in the migration pattern it is clear that the complexes are heterotypic, and probably dimeric (a 2 : 2 tetrameric complex is unlikely, although it cannot be ruled out). A plot of charge versus pH (not shown) explains the migration patterns for the peptides at pH 3.8. Charges were calculated using PROTEIN CALCULATOR v3.3 (http://www.scripps.edu/~cdputnam/protcalc.html).

**Table 1.** Kinetic folding data associated with each of the identifiable transitions. The columns represent the folding data associated with the 2U-to-$I_2$ transition, the $I_2$-to-$F_2$ transition and the $F_2$-to-2U transition. The rate constants and *m*-values associated with these transitions are derived from Eqns 6–9 and are displayed in Fig. 4.

| | $k_{f1}$ ($M^{-1}\cdot s^{-1}$) | $m_u$–$m_{t1}$ (cal·mol$^{-1}$ ·$M^{-1}$) | $k_{f2}$ ($s^{-1}$) | $m_I$–$m_{t2}$ (cal·mol$^{-1}$ ·$M^{-1}$) | $k_{u1}$ ($s^{-1}$) | $m_f$–$m_{t2}$ (cal·mol$^{-1}$ ·$M^{-1}$) | $k_{u2}$ ($s^{-1}$) | $m_I$–$m_{t1}$ (cal·mol$^{-1}$ ·$M^{-1}$) | $\Delta G_{kin}$ (kcal ·mol$^{-1}$) |
|---|---|---|---|---|---|---|---|---|---|
| cJun–FosW | 5.8e$^6$ ± 1.3e$^6$ | −1.4 ± 0.2 | 2.3 ± 0.5 | −0.2 ± 0.2 | 0.046 ± 0.01 | 1.0 ± 0.1 | 0.92[a] | 4.2[b] | ?? |
| cJun(R)–FosW(E) | 7.1e$^6$ ± 1.6e$^6$ | −1.9 ± 0.2 | 4.0 ± 0.7 | −1.0 ± 0.1 | 0.0001 ± 0.0001 | 2.5 ± 0.21 | 0.0018 ± 0.0002 | 1.41 ± 0.027 | −19.0 |

[a] Estimated from kinetic parameters; $\Delta G$ derived from thermal denaturation data.
[b] Deduced assuming $m_{eq}$ = −6.8 as for the Jun(R)–FosW(E) molecule (see *m*-values).

complexes (1.47–3.22 × $10^6$ $M^{-1}\cdot s^{-1}$, equivalent to a $k_{app}$ of 29–64 $s^{-1}$ [24]). This is probably because cFos contains fewer hydrophobic side chains in the core than cJun. This initial rate was followed by a slower unimolecular phase (2.3 $s^{-1}$) before arriving at the folded state. In addition, the unfolding rate was slow ($k_{u1}$ = 0.046 $s^{-1}$) relative to the cFos–JunW complexes previously described (0.26–1.31 $s^{-1}$ [24]). The second unfolding rate ($k_{u2}$) was not observed, but can be estimated to be 0.92 $s^{-1}$ based on the $\Delta G_{eq}$ value determined by thermal denaturation. This value is fast and therefore consistent with the detection of only one unfolding phase. All of these rates combine to give an overall equilibrium stability that was higher for the cJun–FosW complex relative to the cFos–JunW complex [20].

### cJun(R)–FosW(E)

This dimer exhibited two detectable folding phases ($k_{f1}$ = 7.1 × $10^6$ $M^{-1}\cdot s^{-1}$, $k_{f2}$ = 4.0 $s^{-1}$) and two unfolding phases ($k_{u1}$ = 0.0001 $s^{-1}$, $k_{u2}$ = 0.0018 $s^{-1}$). The bimolecular rate is faster than for the parent molecule, probably reflecting the more rapid formation of collision complexes when electrostatic steering is a factor [33,34]. More importantly, cJun(R)–FosW(E) has decelerated unfolding rates relative to the cJun–FosW parent molecule. This was predicted from previous data, where it was asserted that the intricate formation of salt bridges is probably a late folding event [24]. However, it should be noted that this effect was observed for both detectable unfolding rates, implying that longer range charge effects are also manifesting themselves. Indeed, the initial unfolding rate constant, $k_{u1}$, is some 460 times slower than the corresponding unfolding rate ($k_{u1}$) for cJun–FosW, and $k_{u2}$ some 500 times (based on the calculated $k_{u2}$ for cJun–FosW). Collectively this amounts to an electrostatically stabilized dimer that folds at a rate that is only slightly faster than that of the cJun–FosW parent molecule, but unfolds at much slower rates than cJun–FosW. The combined factors in the unfolding rates give a stabilization of 460 × 500.

### Helical propensities

Inspection by the helical content prediction algorithm AGADIR [30–32] upon cJun in isolation predicted its helicity as 4.2% and for Jun(R) 6.3%. In contrast, FosW previously selected from a semirandomized library using PCA was of comparatively high helical propensity (46%), with the FosW(E) peptide of modest helical content (11.8%). Collectively these values imply that in this study helicity is not a major determinant in overall interaction stability.

**Table 2.** Equilibrium free energy data derived from thermal unfolding profiles at 20 μM total peptide concentration and extrapolated to 293K (see also Fig. 2). In addition, thermal values were collected at 150 μM total peptide concentration using a reference temperature of 293K. In both instances, a plot of ln$K_D$ versus temperature using fraction unfolded ($F_U$) data from the transition point only was used to give the best estimate of ln$K_D$ at the reference temperature [this was not possible for cJun(R)–FosW(R) at 150 μM because of its high stability].

| | $T_m$ at 20 μM (and derived $\Delta G$ at 293K) | $T_m$ at 150 μM (and derived $\Delta G$ at 293K) | bCIPA $T_m$ values (150 μM) | Base optimized weights (BOW) |
|---|---|---|---|---|
| cJun–FosW | 56 °C (−11.4 kcal·mol$^{-1}$) | 63 °C (−12.4 kcal·mol$^{-1}$) | 70 °C | 41.4 |
| cJun(R)–FosW(E) | 82 °C (−18 kcal·mol$^{-1}$) | 98 °C (not determined) | 94 °C | 55.6 |

**Table 3.** Core and electrostatic energetic contributions to coiled coil stability. cJun–FosW and cJun(R)–FosW(E) share the same core residues (which contribute an estimated −23.0 kcal·mol$^{-1}$ to the free energy of folding [48]). It is therefore possible to elucidate the 'electrostatic' residues' contribution to coiled coil stability, relative to the cJun–FosW parent protein [29]. The individual predicted increase in stability from electrostatic contributions relative to cJun–FosW was relatively small ($\Delta\Delta G$ = −8.7 − −4.9 = −3.8 kcal·mol$^{-1}$). However, the actual stability increase observed was rather larger, and these experimental data are in close agreement with stability predictions made by bCIPA. The scorings given to the $g_i$–$e'_{i+1}$/$e_{i+1}$–$g'_i$ pairing are shown in parentheses. Single letter amino acid codes are given (e.g. ER = Glu-Arg).

| | cJun–FosW | cJun(R)–FosW(E) |
|---|---|---|
| $g_1$–$e'_2$ | EK = −1.15 (−1.5) | ER = −1.45 (−1.5) |
| $g_2$–$e'_3$ | RA = −0.45 (−0.5) | ER = −1.45 (−1.5) |
| $g_3$–$e'_4$ | ER = −1.45 (−1.5) | ER = −1.45 (−1.5) |
| $e_2$–$g'_1$ | EK = −1.15 (−1.5) | RE = −1.45 (−1.5) |
| $e_3$–$g'_2$ | RQ = −0.7 (−1) | RE = −1.45 (−1.5) |
| $e_4$–$g'_3$ | QT = ? (?) | RE = −1.45 (−1.5) |
| Total | −4.9 + TQ | −8.7 |

### *m*-values

*m*-values can be used as a measure of the protein-folding reaction coordinate, by providing an estimate of the degree of solvent exposure of a given state in the folding reaction [35–37]. Thus, values for $m_u$, $m_{t1}$, $m_I$, $m_{t2}$ and $m_f$ are *m*-values associated with each of the identifiable states of the folding pathway and relate to the amount of solvent-exposed surface area in each of these states (see Materials and methods). This can be done for all five states in the folding/unfolding pathway of cJun(R)–FosW(E) and the *m*-value associated with the $I_2$-to-2U transition for cJun–FosW can be estimated based on the $m_{eq}$ value (−6.8) taken from the cJun(R)–FosW(E) mutant (Table 1, Fig. 5). On the basis of these data, it appears that the parent cJun–FosW molecule acquires the bulk of its structure (61%) between t1 and $I_2$ (which is not populated in the unfolding direction, see Table 1). Indeed, the $k_{u2}$ step was calculated to be fast (0.92 s$^{-1}$) when calculated from the $\Delta G_{F/U}$ and the identifiable rate constants. The cJun(R)–FosW(E) mutant, however, in which the intermediate state is populated in both directions, sees a large amount of solvent exclusion in the initial U-to-t1 step (28%) and an even larger amount of solvent exclusion in the final $t_2$-to-F folding step (37%), consistent with the formation of the native state.

## Discussion

PCA [20] and phage display [25] have been previously combined with semirational design to generate peptides that form a range of coiled coil interactions and that could be used to block biologically relevant interactions. This was previously confirmed using thermal melting data, gel shift assays, native gels and covalent coupling followed by size exclusion chromatography. The stringency of PCA selection has additionally been increased by using the Competitive and Negative Design Initiative to confer added specificity in addition to stability on the resulting protein–protein interaction. In this way, the energy gap between the desired and nondesired species is intentionally maximized. The Competitive and Negative Design Initiative was demonstrated on a library in which the *a*, *e* and *g* residues of a Jun-based library were semirandomized [21]. More recently, the free energy of the folding pathway of cFos–JunW variants has been dissected to glean new rules that will aid in the future design of stable and specific antagonists [24]. This involved a comparison of PCA- and phage display-selected peptides from the same library and which reassuringly differed from each other in only two of 10 semirandomized positions. These consisted of a mutation that predominantly affected the folding rate by improving hydrophobicity via enhanced core shielding and helical propensity via intramolecular electrostatics, and a mutation that improved intermolecular electrostatic interactions to decelerate the unfolding rate of preformed coiled coils.

On the basis of these initial findings, it appeared that electrostatic interactions make large energetic contributions to both folding/association rates and, more interestingly, unfolding/dissociation rates. Furthermore, the introduction of multiple electrostatics can probably be used to maximize the stability of the desired interaction and improve specificity, provided that alternative favourable interactions are not present in competing homologues. Indeed, Grigoryan *et al.* [38] recently devised an algorithm to analyse and optimize specificity/stability tradeoffs in protein design, and found that *e/g* as well as *g/a* residues make significant contributions to specificity. It was also hypothesized that helical propensity plays a dominant role in folding by conferring helices that are in a dimerization competent state prior to collision, as was previously speculated for the Jun–Fos system [20,24]. For the four monomers in this study, however, AGADIR [30–32] predicts that only the PCA-selected FosW is of notably high helical propensity (data not shown), suggesting that this factor is less important than electrostatic and hydrophobic contributions once a critical helical threshold is reached. Perhaps the contribution to coiled coil stability is negligible once this intrinsic critical level of helicity has been surpassed.

The folding of designed pairs was observed in which six pairs of optimized electrostatic [cJun(R)–FosW(E)] residues have been introduced to robustly ascertain the contribution of enhanced intermolecular electrostatic interactions to overall equilibrium stability. More importantly, it was necessary to establish how these effects are manifested in the kinetic parameters that dictate overall stability, and the cumulative effect of introducing these multiple electrostatic pairs. The most striking finding of this study was the large equilibrium stability increase afforded by the introduction of these pairs (6.6 kcal·mol$^{-1}$ of increased stability). This was evident in the folding pathway for the Arg-Glu mutant via both a slightly faster folding rate and a vastly decelerated overall unfolding rate, relative to the cJun–FosW parent molecule (see Table 1, Fig. 4). It had been previously implied from a single point mutation within a related cFos–JunW that an improved electrostatic contact exerted its effect primarily on the unfolding rate [24], but it was necessary to prove this vigorously for the Jun–Fos system in general.

Having now established this unequivocally, the above findings are of particular importance in our ability to engineer increased protein–protein interaction stability at will; in particular, the ability to increase stability by kinetic design. For example, by achieving this predominantly by decelerating unfolding/dissociation rates (which in our case are tightly coupled; see Fig. 6), this will correlate with an increased 'residency time' for the protein–antagonist complex. It has been speculated that the longer the antagonist–target interaction prevails, the higher the efficacy of the antagonist is likely to be [39,40]. In this respect, having two high barriers between the fully folded state and the free dissociated species will serve to amplify this effect. Although the first bimolecular barrier to folding would appear to be small, the second barrier relating to the unimolecular $k_{f2}$ step seems much higher. We interpret this second step as representing chain alignment, rearrangement and optimization of noncovalent bonds. Although the possibility of strand exchange from homodimer to heterodimers cannot be ruled out, the first unfolding phase is much slower than the second for the cJun(R)–FosW(E) mutant and both rates are independent of peptide concentration.

Indeed, from a design perspective, a protein–protein interaction with a very low dissociation rate is highly desirable. Consequently, changes to the antagonist that can increase its 'residency time' will help in optimizing drug discovery efforts. It has been further suggested that by maximizing the dissociative half-life, one can approach the ultimate physiological inhibition, by which recovery from inhibition can only occur as the

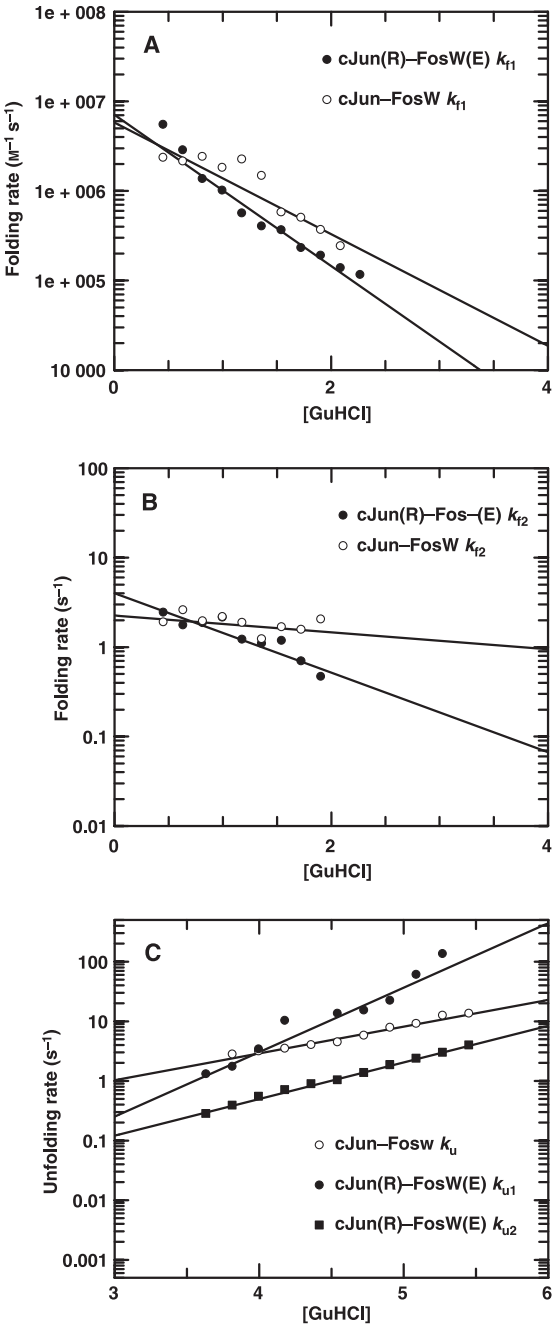


**Fig. 4.** GuHCl dependence of the rate constants for refolding (A, $k_{f1}$; B, $k_{f2}$) and unfolding (C, $k_{u1}$ and $k_{u2}$). Shown are the kinetic folding and unfolding data for cJun–FosW (empty circles). Also shown are folding (A, B, filled circles) and unfolding (C, filled circles and filled squares) data for cJun(R)–FosW(E). Values for $k_{u2}$ are somewhat prone to error. This error results from the large differences in the transient amplitude for $k_{f1}$ relative to $k_{f2}$ ($\sim$ 14.5 versus 2.1), meaning that although the initial fast rate can be accurately determined, the second cannot [see (B)]. Lines represent global fits to the data, with each data point being the average of at least three kinetic transients. In the case of (A), $k_{app}$ has been corrected for peptide concentration according to Eqn 4b.

result of new target synthesis. Consequently, if one is able to concomitantly increase the rate at which the protein–antagonist binary complex is formed, the peptides will have particularly favourable $K_D$ values. Accelerated on-rates will result in allowing antagonists to be administered at lower doses, easing issues such as production cost and toxicity in the process.

Some previous studies on coiled coil proteins have suggested that electrostatic interactions contribute to stability via both association and dissociation rates [41,42], whereas other studies have argued that the contribution is predominantly via dissociation rates [24,43]. Indeed, on the basis of the data presented here, a coiled coil with maximized electrostatic interactions that can decelerate unfolding/dissociation while conferring specificity would appear to present a valid design strategy. Copeland *et al.* [39] have contended that this is an underappreciated model of drug action, arguing that as long as the receptor–ligand association rate is suitably fast (for *in vivo* function), the duration of efficacy depends more critically on the dissociation rate constant. On the basis of the findings of this study, the best way to ensure this is to engineer refined electrostatic intermolecular contacts into the protein–ligand complex, which will increase complex stability predominantly via a decelerated dissociation rate.

To quantify the above effect in the system described here, the effective rate of dissociation to free peptide can be calculated on the basis of net rate constants and reaction partitions [44] (Fig. 6). In the coiled coil kinetics system, the net rate of dissociation ($k$) is defined by the first off-rate ($k_{u1}$) multiplied by the partition for the second step: $k_{u2}/(k_{f2} + k_{u2})$, hence:

$$k = k_{u1} \cdot k_{u2}/(k_{f2} + k_{u2}) \quad (1)$$

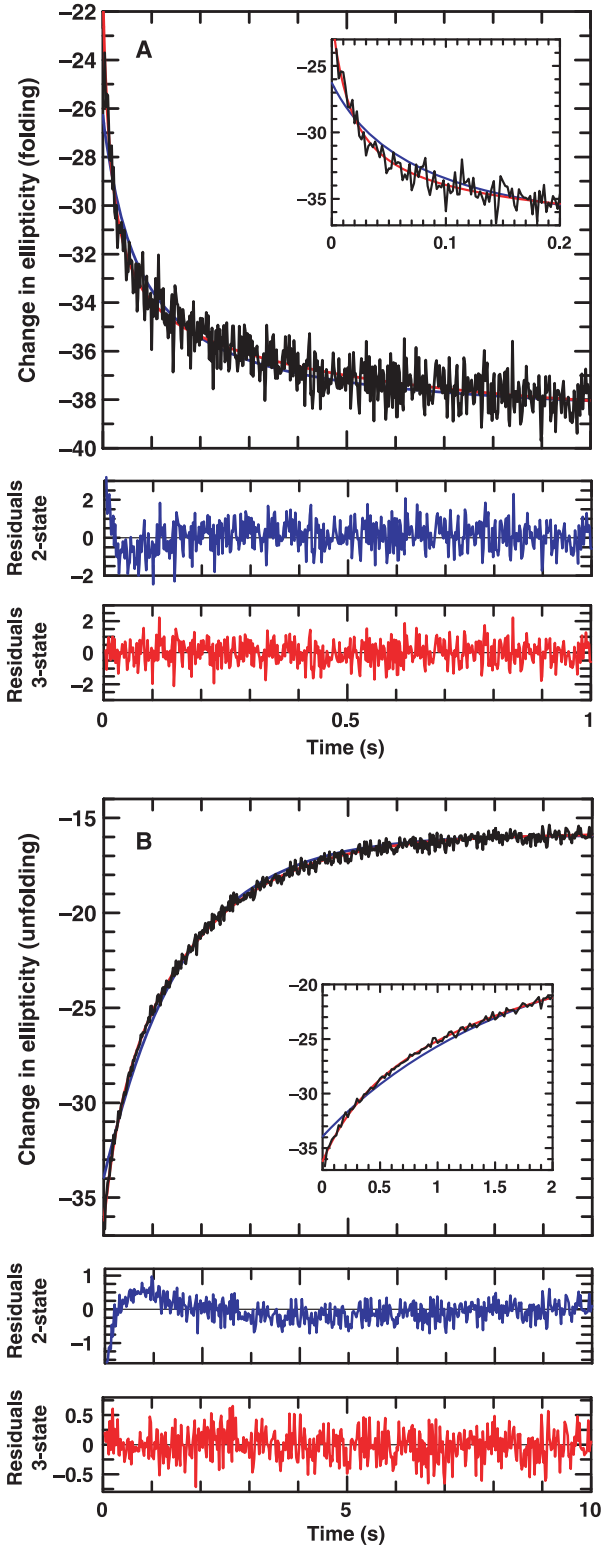


**Fig. 5.** Folding and unfolding behaviour of the cJun(R)–FosW(E) variant. Solid lines represent the two- and three-state fits to folding data in 0.64 M GuHCl (A). Also shown are the residuals for two-state (blue) and three-state (red, Eqn 4a) fits to the data. Only the latter is a satisfactory fit. Shown inset are the two-state and three-state fits for the first 200 ms of the transient, with the latter clearly providing the better fit. Likewise, (B) shows an unfolding transient in 4.0 M GuHCl. In this case, a single exponential fit (Eqn 5a) is insufficient to describe unfolding data and a double exponential fit (red, Eqn 5b) is required. Below are the residuals for these fits. In both reactions the earliest measurable signal is equal to the value for the initial state measured separately, indicating that there is little change in ellipticity in the initial 5 ms of instrument deadtime. Again, the inset shows two-state and three-state fits to the first 2 seconds of the transient, with the latter clearly providing the better fit. For the parent molecule the single exponential in the unfolding direction can be explained by the low transition state barrier (t1) between 2U and $I_2$ relative to the second transition state barrier (t2). This means that $k_{u1} << k_{u2}$, and that $k_u$ therefore approximates to $k_{u1}$ (see Eqn 3). Experimental conditions for folding/unfolding reactions are given in the Materials and methods section.

For the parent coiled coil, the net dissociation rate can be calculated to be $1.3 \times 10^{-2}$ s$^{-1}$, whereas for the electrostatically stabilized version it is $4.5 \times 10^{-8}$ s$^{-1}$. This represents a change in residency time from just over a minute to almost 9 months. Thus, although mutations provide information on the overall equilibrium free energy, it is also important to dissect this overall value into its component kinetic steps. The findings of this study are therefore of interest to the protein design field in general, but also inform upon how to fast track the design of peptides with the potential to serve as leads for the design and synthesis of therapeutic mimetics.

## Materials and methods

### Peptide synthesis and purification

Peptides were synthesized by Protein Peptide Research (Fareham, UK) and subsequently purified to over 98% purity using RP-HPLC with a Jupiter Proteo column (4 μm particle size, 90 Å pore size, 250 × 10 mm; Phenomenex) and a gradient of 5–50% acetonitrile (0.1% trifluoroacetic acid) in 50 min at 1.5 mL·min$^{-1}$. Correct masses were verified by electrospray MS. The following peptides: cJun ASIARLEEKVKTLKAQNYELASTANMLREQVAQLGAP; FosW ASLDELQAEIEQLEERNYALRKEIEDLQKQLEKLGAP; FosW(E) ASLDELEAEIEQLEEENYALEKEIEDLEKELEKLGAP; cJun(R) ASIARLRERVKTLRARNYELRSRANMLRERVAQLGAP were synthesized as amidated and acetylated peptides and contained N- and C-capping motifs (underlined) for improved helix stability and solubility. Peptide concentrations were determined in water using absorbance at 280 nm with an extinction coefficient of 1209 M$^{-1}$·cm$^{-1}$ [45] corresponding to a Tyr residue inserted into a solvent-exposed *b3* heptad position.

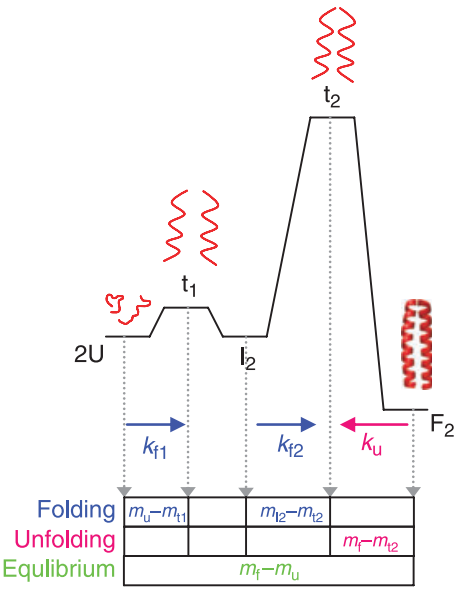


**Fig. 6.** Free energy diagram highlighting the identifiable steps in the folding pathway. Rate constants are determined by the relative heights of transition state barriers. When the first transition state (t1) is significantly smaller than the second then two forward phases and one unfolding phase are observed (e.g. cJun–FosW). In contrast, when the transition states are of approximately equal height then two forward and two reverse phases are observed [e.g. cJun(R)–FosW(E)]. *m*-values associated with the transitions (according to Eqns 6–9) are also shown, as is the overall *m*-value from equilibrium. Shown above are schematics of the molecule; at the denatured state the helices are almost entirely random coil.

### Equilibrium stability data

Spectra and thermal melts were performed at 20 and 150 μM total peptide concentration in 10 mM potassium phosphate, 100 mM potassium fluoride, pH 7, using an Applied Photophysics Chirascan CD instrument (Leatherhead, UK). The temperature ramp was set to stepping mode using 1 °C increments and paused for 30 s before measuring ellipticity. Melting profiles (see Fig. 2) were ≥ 95% reversible with equilibrium denaturation curves fitted to a two-state model to yield $T_m$:

$$\Delta G = \Delta H - (T_A/T_m) \times [\Delta H + R \times T_m \times \ln(P_t)] + \Delta C_p \times [T_A - T_m - T_A \times \ln(T_A/T_m)] \quad (2)$$

where $\Delta H$ is the change in enthalpy, $T_A$ is the reference temperature, $R$ is the ideal gas constant (1.9872 cal·mol$^{-1}$·K$^{-1}$), $P_t$ the total peptide concentration (either 150 or 20 μM) and $\Delta C_p$ the change in heat capacity. Melting profiles for heterodimers are clearly distinct from averages of constituent homodimeric melts (also shown in the native gel analysis; Fig. 3), indicating that helices are dimerizing in an apparent two-state process. Protein-folding studies have demonstrated that for GCN4, a yeast homologue of AP-1, both binding and dissociation of dimers is tightly coupled with folding/unfolding of the individual helices, and is well described by a simple two-state model [46,47]. Our own previous studies have shown that for cFos–JunW-based peptides, folding occurs via an intermediate that is undetectable in denaturation experiments [24]. To obtain the most accurate value for the free energy of unfolding in water ($\Delta G_{F \rightarrow U(W)}$), values for $F_U$ were taken from the transition zone of the denaturation profiles (see Fig. 2) and converted to $K_D$ (see Eqn 5 in [24]) and a linear fit was carried out (Fig. 2B). This is because the signal to noise ratio is at its lowest where the change in intensity is at its greatest, and is achieved by plotting the derived $\ln(K_D)$ as a function of temperature. A linear fit is used to extrapolate to the free energy of unfolding in water ($\Delta G_{F \rightarrow U(W)}$) at 293K, in

accordance with the linear extrapolation method (see also Table 2).

## Stopped-flow CD

Folding measurements (Fig. 4A, B) were initiated by mixing a 220 μM solution of denatured peptide containing 10 mM potassium phosphate, 100 mM potassium fluoride and 5.0 M GuHCl (pH 7.0) against 10 volumes of the given concentration of GuHCl at 293K in a Chirascan stopped-flow CD apparatus (Applied Photophysics) to give a postmix peptide concentration of 20 μM. The initial folding rate, $k_{f1}$, was calculated from $k_{app}$ according to Eqn 4b. The relationship between the first folding phase and the protein concentration has been shown to be linear within the 5–20 μM range [24]. A wavelength of 222 nm was selected using entrance and exit slit widths of 4 mm. The postmix concentration of GuHCl was calculated according to the following: [5 M + (premix [GuHCl] * 10)]/11. Folding measurements were taken between 0.45 and 2.3 M postmix GuHCl concentrations (see Fig. 4A, B), a range in which the unfolding rate was not expected to contribute significantly. For the unfolding reactions, a 220 μM solution of folded peptide in 10 mM potassium phosphate, 100 mM potassium fluoride pH 7.0 was mixed against 10 volumes of an appropriate concentration of GuHCl at 293K and the postmix GuHCl concentration calculated according to the following: (premix [GuHCl] * 10)/11. Unfolding measurements were taken between 3.6 and 5.5 M GuHCl (see Fig. 4C), where folding was not predicted to contribute significantly. All concentrations of GuHCl dilutions were determined by refractometry. The resulting data points are the result of at least three kinetic transient averages.

## Kinetic data analysis

Kinetic data were fitted to the following three-state model:

$$2U \underset{k_{u2}}{\overset{k_{f1}}{\rightleftharpoons}} I_2 \underset{k_{u1}}{\overset{k_{f2}}{\rightleftharpoons}} N_2 \quad (3)$$

In this model, $I_2$ represents a dimeric intermediate that was detectable either via folding data only (cJun–FosW) or by both folding and unfolding data [cJun(R)–FosW(E)]. In the folding direction, two phases [cJun–FosW and cJun(R)–FosW(E); Eqn 4a] were observed (see Table 1). This is consistent with a dimeric intermediate state that is transiently populated during folding. Evidence for this intermediate is supported by the fact that the first folding constant ($k_{f1}$) is bimolecular, being dependent upon the concentration of denatured peptide [24], which informs that the intermediate state is dimeric. The second folding rate ($k_{f2}$) is more prone to error than the first ($k_{f1}$), owing to its small relative amplitude (with an average of 14.5 versus 2.10). It is clear, however, that the rate constants for these two folding events differ by over five orders of magnitude and have consequently been fitted as uncoupled events. The folding data were fitted according to the following time-dependent decrease in ellipticity (increase in helicity):

Three-state folding:

$$\theta(t) = \theta_0 + \theta_1 \cdot \left(\frac{1}{1 + (k_{app} \cdot t)}\right) + (\theta_2 \cdot \exp(-k_{f2} \cdot t)) \quad (4a)$$

where:

$$k_{app} = k_{f1} \cdot Pt \quad (4b)$$

where $\theta_0$ is the final ellipticity, $\theta_1$ is the change in ellipticity associated with the first folding transition, $\theta_2$ is the change in ellipticity associated with the second folding transition, $k_{app}$ is the apparent rate constant for the first folding transition at a given peptide concentration, $k_{f2}$ is the rate constant associated with the second folding transition, and $t$ is time.

In the unfolding direction, either one or two exponentials are required to fit the kinetic transients, such that the barrier between $F_2$ and 2U is:

Two-state unfolding:

$$\theta(t) = \theta_0 + \theta_1 \cdot (1 - \exp(-k_{u1} \cdot t)) \quad (5a)$$

Three-state unfolding:

$$\theta(t) = \theta_0 + A_1 \cdot (1 - \exp(k_{u1} \cdot t)) + A_2 \cdot (1 - \exp(-k_{u2} \cdot t)) \quad (5b)$$

For the two-state model (Eqn 5a), $k_{u1}$ is slow relative to $k_{u2}$ because of the small size of the transition state barrier that is associated with the second unfolding transition between $I_2$ and 2U (see Fig. 5), and consequently the overall $k_u$ approximates to $k_{u1}$ [24]. This unimolecular reaction is not influenced by the concentration of dimer prior to unfolding and is therefore independent of protein concentration. This model is supported by equilibrium data collected at 20 μM where no intermediate is detectable (Fig. 2); taken together this indicates that the folding barrier between the unfolded state and intermediate is easily surmounted in both directions. For the three-state model, the data were fit as uncoupled events according to Eqn 5b. Finally, data can be fitted as a function of denaturant concentration to yield the kinetic constants for folding and unfolding in 0 M denaturant (w) according to Eqns 6–9:

$$\ln k_{f1} = \ln k_{f1(w)} + (m_u - m_{t1}) \cdot D \quad (6)$$

$$\ln k_{f2} = \ln k_{f2(w)} + (m_I - m_{t2}) \cdot D \quad (7)$$

$$\ln k_{u1} = \ln k_{u1(w)} + (m_f - m_{t2}) \cdot D \quad (8)$$

$$\ln k_{u1} = \ln k_{u2(w)} + (m_I - m_{t1}) \cdot D \quad (9)$$

where $\ln k_{f1}$ and $\ln k_{f2}$ are folding constants associated with first and second transitions, respectively, at any given denaturant concentration, and $\ln k_{u1}$ and $\ln k_{u2}$ are the unfolding

rates associated with the first and second unfolding transitions, respectively, at any given final denaturant concentration. Values for $m_u$, $m_{t1}$, $m_I$, $m_{t2}$ and $m_f$ are *m*-values associated with each of the identifiable states of the folding pathway and relate to the amount of solvent-exposed surface area in each of these states, and thus can be used as a measure of the extent to which the folding reaction has progressed. These equations were used to extrapolate the rate constant and/or free energy of the relevant transition to 0 M denaturant concentration.

### Kinetic studies

The kinetics of folding were fitted to a biphasic equation that assumed a dimeric intermediate (Eqn 4), as reported for cFos–JunW [24]. Evidence for a dimeric intermediate comes from the fact that the kinetic traces show two phases. The first transition was found to be concentration dependent for the peptide range 5–20 μM [24] (see Fig. S1A) and a three-state model was proposed with a dimeric intermediate. For both dimers, acquisition of the first barrier to folding was very fast (Table 1; $\sim 6–7 \times 10^6$ $M^{-1}{\cdot}s^{-1}$ in agreement with previously reported coiled coil folding rates of $4 \times 10^5$ $M^{-1}{\cdot}s^{-1}$ [46] and $2 \times 10^6$ $M^{-1}{\cdot}s^{-1}$ [47]), whereas the second was a first-order event (of $\sim 2–4$ $s^{-1}$; see also Fig. S1B) and that at this concentration (20 μM) the two events are not coupled. Kinetic folding data can be found in Tables S1A and S1C. The unfolding rate displayed only one phase for cJun–FosW and was fitted to a two-state mechanism (Eqn 5a). However, for cJun(R)–FosW(E), fitting to a two-state model did not produce satisfactory residuals and it was necessary to fit as a three-state model (Eqn 5b). In addition, $k_{u2}$ is not dependent upon the concentration of protein, as is consistent with a unimolecular reaction (see Fig. S1C). However, it should be noted that we were unable to rule out the possibility that the complex kinetics result from the transient formation of a homodimeric species prior to the formation of the heterodimer. Kinetic unfolding data can be found in Tables S1B and S1D.

### Native gel electrophoresis

Native gel electrophoresis was necessary to demonstrate that peptides form heteromeric complexes of 1 : 1 stochiometry. To do so, samples of individual peptides as well as equimolar mixtures were diluted two-fold in 0.2% (w/v) methyl green, 20% glycerol, 500 mM β-alanine acetate, pH 3.8. The peptides were loaded to a concentration of 480 μM. Gels contained 7.5% acrylamide in 375 mM β-alanine acetate, pH 3.8. The gel was prerun for 1 h, samples were loaded and the gel was run for a further 3 h at 100 V. During this time it was necessary to reverse the electrodes so that the protein sample ran to the anode. Gels were fixed with 2% glutaraldehyde and stained overnight in 0.2% Coomassie brilliant blue (R-250), 20% acetic acid, before destaining in the same solvent lacking the dye. The calculated overall positive charge on the peptides at pH 3.8 (PROTEIN CALCULATOR v3.3; http://www.scripps.edu/~cdputnam/protcalc.html) was as follows: FosW = 3.2, cJun = 4.4, FosW(E) = 0.2, cJun(R) = 9.2.

### Free energy changes from the literature

Calculated differences between coiled coil values at 37 °C (Table 3) have been previously reported in Krylov *et al.* [29] for electrostatic $g_i$–$e'_{i+1}$ and $e_{i+1}$–$g'_i$ contributions and Acharya *et al.* [48] for hydrophobic *a*–*a*′ contributions. In these publications, free energies were calculated relative to an Ala-Ala pair. It should be noted that these values have been averaged from the data reported for $g/e^{i+1}$ and $e^{i+1}/g$.

## Acknowledgements

The author would like to thank the Royal Society (grant DBA4H00) and the University of Essex Biological Sciences Departmental Research Fund for funding this project. The author would also like to thank Tony Clarke for valuable discussions and critical reading of the manuscript.

## References

1 Yu YB (2002) Coiled-coils: stability, specificity, and drug delivery potential. *Adv Drug Deliv Rev* **54**, 1113–1129.
2 Mason JM & Arndt KM (2004) Coiled coil domains: stability, specificity, and biological implications. *ChemBiochem* **5**, 170–176.
3 Woolfson DN (2005) The design of coiled-coil structures and assemblies. *Adv Protein Chem* **70**, 79–112.
4 Mason JM, Muller KM & Arndt KM (2007) Considerations in the design and optimization of coiled coil structures. *Methods Mol Biol* **352**, 35–70.
5 Wolf E, Kim PS & Berger B (1997) MultiCoil: a program for predicting two- and three-stranded coiled coils. *Protein Sci* **6**, 1179–1189.
6 Schuermann M, Neuberg M, Hunter JB, Jenuwein T, Ryseck RP, Bravo R & Muller R (1989) The leucine repeat motif in Fos protein mediates complex formation with Jun/AP-1 and is required for transformation. *Cell* **56**, 507–516.
7 Shaulian E & Karin M (2002) AP-1 as a regulator of cell life and death. *Nat Cell Biol* **4**, E131–E136.
8 Eferl R & Wagner EF (2003) AP-1: a double-edged sword in tumorigenesis. *Nat Rev Cancer* **3**, 859–868.
9 Hess J, Angel P & Schorpp-Kistner M (2004) AP-1 subunits: quarrel and harmony among siblings. *J Cell Sci* **117**, 5965–5973.

10 Zenz R, Eferl R, Scheinecker C, Redlich K, Smolen J, Schonthaler HB, Kenner L, Tschachler E & Wagner EF (2008) Activator protein 1 (Fos/Jun) functions in inflammatory bone and skin disease. *Arthritis Res Ther* **10**, 201.
11 Wagner EF & Eferl R (2005) Fos/AP-1 proteins in bone and the immune system. *Immunol Rev* **208**, 126–140.
12 Aud D & Peng SL (2006) Mechanisms of disease: transcription factors in inflammatory arthritis. *Nat Clin Pract Rheumatol* **2**, 434–442.
13 Loughlin WA, Tyndall JD, Glenn MP & Fairlie DP (2004) Beta-strand mimetics. *Chem Rev* **104**, 6085–6117.
14 Borghouts C, Kunz C & Groner B (2005) Current strategies for the development of peptide-based anti-cancer therapeutics. *J Pept Sci* **11**, 713–726.
15 Davis JM, Tsou LK & Hamilton AD (2007) Synthetic non-peptide mimetics of alpha-helices. *Chem Soc Rev* **36**, 326–334.
16 Lalezari JP, Henry K, O'Hearn M, Montaner JS, Piliero PJ, Trottier B, Walmsley S, Cohen C, Kuritzkes DR, Eron JJ Jr *et al*. (2003) Enfuvirtide, an HIV-1 fusion inhibitor, for drug-resistant HIV infection in North and South America. *N Engl J Med* **348**, 2175–2185.
17 Lazzarin A (2005) Enfuvirtide: the first HIV fusion inhibitor. *Expert Opin Pharmacother* **6**, 453–464.
18 Sato AK, Viswanathan M, Kent RB & Wood CR (2006) Therapeutic peptides: technological advances driving peptides into development. *Curr Opin Biotechnol* **17**, 638–642.
19 McGregor DP (2008) Discovering and improving novel peptide therapeutics. *Curr Opin Pharmacol* **8**, 616–619.
20 Mason JM, Schmitz MA, Müller KM & Arndt KM (2006) Semirational design of Jun-Fos coiled coils with increased affinity: universal implications for leucine zipper prediction and design. *Proc Natl Acad Sci USA* **103**, 8989–8994.
21 Mason JM, Mueller KM & Arndt KM (2007) Positive aspects of negative design: simultaneous selection of specificity and interaction stability. *Biochemistry* **46**, 4804–4814.
22 Mason JM, Mueller KM & Arndt KM (2008) iPEP: peptides designed and selected for interfering with protein interaction and function. *Biochem Soc Trans* **36**, 1442–1447.
23 Pelletier JN, Campbell-Valois FX & Michnick SW (1998) Oligomerization domain-directed reassembly of active dihydrofolate reductase from rationally designed fragments. *Proc Natl Acad Sci USA* **95**, 12141–12146.
24 Mason JM, Hagemann UB & Arndt KM (2007) Improved stability of the Jun-Fos activator protein-1 coiled coil motif: a stopped-flow circular dichroism kinetic analysis. *J Biol Chem* **282**, 23015–23024.
25 Hagemann UB, Mason JM, Muller KM & Arndt KM (2008) Selectional and mutational scope of peptides sequestering the Jun-Fos coiled-coil domain. *J Mol Biol* **381**, 73–88.
26 O'Shea EK, Lumb KJ & Kim PS (1993) Peptide 'Velcro': design of a heterodimeric coiled coil. *Curr Biol* **3**, 658–667.
27 Gonzalez L Jr, Woolfson DN & Alber T (1996) Buried polar residues and structural specificity in the GCN4 leucine zipper. *Nat Struct Biol* **3**, 1011–1018.
28 Fong JH, Keating AE & Singh M (2004) Predicting specificity in bZIP coiled-coil protein interactions. *Genome Biol* **5**, R11.
29 Krylov D, Barchi J & Vinson C (1998) Inter-helical interactions in the leucine zipper coiled coil dimer: pH and salt dependence of coupling energy between charged amino acids. *J Mol Biol* **279**, 959–972.
30 Munoz V & Serrano L (1994) Elucidating the folding problem of helical peptides using empirical parameters. *Nat Struct Biol* **1**, 399–409.
31 Munoz V & Serrano L (1995) Elucidating the folding problem of helical peptides using empirical parameters. III. Temperature and pH dependence. *J Mol Biol* **245**, 297–308.
32 Munoz V & Serrano L (1995) Elucidating the folding problem of helical peptides using empirical parameters. II. Helix macrodipole effects and rational modification of the helical content of natural peptides. *J Mol Biol* **245**, 275–296.
33 Frisch C, Fersht AR & Schreiber G (2001) Experimental assignment of the structure of the transition state for the association of barnase and barstar. *J Mol Biol* **308**, 69–77.
34 Alsallaq R & Zhou HX (2007) Prediction of protein-protein association rates from a transition-state theory. *Structure* **15**, 215–224.
35 Dill KA & Shortle D (1991) Denatured states of proteins. *Annu Rev Biochem* **60**, 795–825.
36 Matouschek A & Fersht AR (1993) Application of physical organic chemistry to engineered mutants of proteins: Hammond postulate behavior in the transition state of protein folding. *Proc Natl Acad Sci USA* **90**, 7814–7818.
37 Parker MJ, Spencer J & Clarke AR (1995) An integrated kinetic analysis of intermediates and transition states in protein folding reactions. *J Mol Biol* **253**, 771–786.
38 Grigoryan G, Reinke AW & Keating AE (2009) Design of protein-interaction specificity gives selective bZIP-binding peptides. *Nature* **458**, 859–864.
39 Copeland RA, Pompliano DL & Meek TD (2006) Drug-target residence time and its implications for lead optimization. *Nat Rev Drug Discov* **5**, 730–739.
40 Tummino PJ & Copeland RA (2008) Residence time of receptor-ligand complexes and its effect on biological function. *Biochemistry* **47**, 5481–5492.

41 Durr E, Jelesarov I & Bosshard HR (1999) Extremely fast folding of a very stable leucine zipper with a strengthened hydrophobic core and lacking electrostatic interactions between helices. *Biochemistry* **38**, 870–880.
42 Meisner WK & Sosnick TR (2004) Fast folding of a helical protein initiated by the collision of unstructured chains. *Proc Natl Acad Sci USA* **101**, 13478–13482.
43 Knappenberger JA, Smith JE, Thorpe SH, Zitzewitz JA & Matthews CR (2002) A buried polar residue in the hydrophobic interface of the coiled-coil peptide, GCN4-p1, plays a thermodynamic, not a kinetic role in folding. *J Mol Biol* **321**, 1–6.
44 Cleland WW (1975) Partition analysis and the concept of net rate constants as tools in enzyme kinetics. *Biochemistry* **14**, 3220–3224.
45 Du H, Fuh RA, Li J, Corkan A & Lindsey JS (1998) PhotochemCAD: a computer-aided design and research tool in photochemistry. *Photochem Photobiol* **68**, 141–142.
46 Zitzewitz JA, Bilsel O, Luo J, Jones BE & Matthews CR (1995) Probing the folding mechanism of a leucine zipper peptide by stopped-flow circular dichroism spectroscopy. *Biochemistry* **34**, 12812–12819.
47 Sosnick TR, Jackson S, Wilk RR, Englander SW & DeGrado WF (1996) The role of helix formation in the folding of a fully alpha-helical coiled coil. *Proteins* **24**, 427–432.
48 Acharya A, Rishi V & Vinson C (2006) Stability of 100 homo- and heterotypic coiled-coil a-a' pairs for ten amino acids (A, L, I, V, N, K, S, T, E, and R). *Biochemistry* **45**, 11324–11332.

## Supporting information

The following supplementary material is available:
**Fig. S1.** Protein concentration dependence upon the rates of folding and unfolding.
**Table S1.** Kinetic data.

This supplementary material can be found in the online version of this article.

Please note: As a service to our authors and readers, this journal provides supporting information supplied by the authors. Such materials are peer-reviewed and may be re-organized for online delivery, but are not copy-edited or typeset. Technical support issues arising from supporting information (other than missing files) should be addressed to the authors.